Physica B 459 (2015) 12–15

Contents lists available at ScienceDirect

Physica B

journal homepage: www.elsevier.com/locate/physb

A comparative study of size-dependent magnetoresistance and Hall resistance of Sb_2Te_3 nanoflakes

Ping-Chung Lee [a,b], Yi-Chi Huang [a,c], C.H. Chien [a,b], F.Y. Chiu [a], Y.Y. Chen [a,d], Sergey R. Harutyunyan [a,e,*]

[a] Institute of Physics, Academia Sinica, Nankang, Taipei 115, Taiwan
[b] Department of Engineering and System Science, National Tsing Hua University, Hsinchu 300, Taiwan
[c] Department of Physics, National Central University, Chung-Li 320, Taiwan
[d] Graduate Institute of Applied Physics, National Chengchi University, Taipei 106, Taiwan
[e] Institute for Physical Research, NASRA, Ashtarak 0203, Armenia

ARTICLE INFO

Article history:
Received 30 September 2014
Received in revised form
14 November 2014
Accepted 21 November 2014
Available online 24 November 2014

Keywords:
Magnetoresistance
Hall effect
Topological insulator

ABSTRACT

Single crystal Sb_2Te_3 topological insulator nanoflakes with the thickness of 25 nm and 456 nm were synthesized via vapor phase deposition method. The Hall resistance and magnetoresistance of the nanoflakes have been measured at temperatures 2 K and 300 K in the fields up to 9 T. The magnetoresistance and Hall resistance of the nanoflakes demonstrate significant differences, so that despite ordinary magnetoresistance and Hall effect obtained for 25 nm sample 450 nm nanoflake demonstrates unusual magnetoresistance and nonlinear Hall resistance. The sense of curvature of both $R_{xx}(B)$ and $R_{xy}(B)$ dependences is inversed at high temperature. The experimental data have been analyzed in the frame of a multichannel transport model. The difference in the behavior is attributed to the existence of the charge carriers with high and low mobility, as well as to their relative contribution (which varies depending on the temperature) to the magneto-transport of the nanoflakes.

1. Introduction

Topological insulators (TIs) represent a new state of quantum matter and attract heightened interest due to unique properties associated with the metallic gapless surface states. The unique surface states having spin-polarized nature with the spin-up and spin-down currents (protected by time-reversal symmetry) originate as the consequence of strong spin–orbit coupling, inherent for this class of materials [1]. TIs are considered as an ideal base for spintronics, quantum computations and other applications [2,3]. Several quantum transport phenomena in 3D TI such as Shubnikov de Hass (SdH) oscillations, weak antilocalization (WAL), universal conductance fluctuation (UCF), Aharonov–Bohm, Atshuler–Aronov–Spivak and Aharonov–Casher effects have already been observed in nanowires, nanoribbons and thin films [4–10]. Other interesting phenomena are the nonsaturating and linear magnetoresistance as well as an anomalous behavior of Hall resistance detected in TIs [11–17]. It has been suggested [14,15] that linear-like MR response arises from the linear Dirac surface dispersion, which according to the quantum theory of linear MR (LMR) developed by Abrikosov should result in such a phenomenon [16]. Some studies have also suggested that a modified Hikami–Larkin–Nagaoka model of quantum phase coherence can describe the magnetic-field-dependent MR [17]. The anomalous Hall effect was previously discovered in the ferromagnetic conductors and is induced by the spin-dependent scattering of charge carriers [18]. The origin of nonlinear Hall resistance in TIs was attributed to the topological nature i.e. to the contribution of the surface states and results mainly from the anomalous Hall effect of Dirac theory [11,15].

In this paper we report on fabrication of single crystalline antimony telluride Sb_2Te_3 nanoflakes and study size-dependent magnetoresistance and Hall resistance in order to reveal contribution of the surface states. The Sb_2Te_3 compound is known as *p*-type thermoelectric semiconductor and recently it has been predicted and confirmed that the compound is three-dimensional (3D) topological insulator (TI) [19,20]. The multivalley valence band of Sb_2Te_3 consists of the upper valence band, UVB (light effective mass holes) and lower valence band, LVB (heavy effective mass holes) [21]. Taking into account that the observation of the effects related to contribution of the topological surface states requires decrease of the bulk response (reduced thickness), we

* Coresponding author at: Institute for Physical Research, NASRA, Ashtarak 0203, Armenia.
E-mail address: sergeyhar56@gmail.com (S.R. Harutyunyan).

http://dx.doi.org/10.1016/j.physb.2014.11.088
0921-4526/

have chosen two samples, differing greatly in thickness ("ultra-thin" −25 nm and "bulk" – 450 nm) for comparison.

2. Experimental results

Single crystalline Sb_2Te_3 nanoflakes of various thickness were grown by vapor phase deposition on SiO_2/Si substrate from stoichiometric polycrystalline Sb_2Te_3 source material. The detailed information is published elsewhere [10,22,23]. Two nanoflakes with the thickness 25 nm and 456 nm were selected for measurements. The Sb/Te atomic ratio defined by means of Energy Dispersive X-ray Spectroscope corresponds to $(41 \pm 1)/(59 \pm 1)$ which is the same for both samples. The leading wires of Au/Ni were fabricated using electron beam lithography. The samples selected for the measurements had symmetrically positioned Hall contacts.

Transport measurements were carried out by four-probe method in physical properties measurement system (PPMS) with magnetic fields up to 9 T at temperatures of 2 K and 300 K. The magnetoresistance was defined as $(100\%) \times (R_B - R_0)/R_0$, where $R_B = R(B)$ is the resistance in magnetic field and R_0 is the resistance without magnetic field. The probe current was directed in crystallographic *ab* plane and MR was investigated for transverse directions of the magnetic field induction vector **B**. The Hall voltage was taken as half the difference between two opposite directions of the induction vector **B.**

The temperature dependence of the resistance $R(T)$ of Sb_2Te_3 nanoflakes was measured in the temperature range from 2 K to 300 K. The results for normalized resistance $R(T)/R(300\ \mathrm{K})$ are illustrated in Fig. 1. The resistance of both samples is showing metallic behavior and the thicker the sample is, the stronger the temperature dependence is observed. Such a correlation with the size of the samples appears due to the increasing of the degree of disorder (i.e. increased scattering on boundaries and defects) with decreasing the thickness of the nanoflakes. This reflects the fact that reducing the size of the sample leads to an increase of the relative contribution from the surface of the nanoflake heavily occupied by defects. The defects in the Sb_2Te_3 compound consist of Sb vacancies and Sb_{Te} antisite defects which are responsible for the generation of holes and thus an increase in defects leads to an increase in the concentration of holes. The magnetic field dependences of the transverse resistance R_{xy} of our Sb_2Te_3 nanoflakes are depicted in Fig. 2. While the transverse resistance R_{xy} of 25 nm nanoflake is practically linear at both 2 K and 300 K temperatures the transverse resistance R_{xy} of 450 nm nanoflake is nonlinear and the sense of curvature of the $R_{xy}(B)$ line is inversed at 300 K. Based on the Hall resistance results we deduced the values of the mobility $\mu = R_H/\rho = 0.0145\ \mathrm{m^2/V};\ 0.0075\ \mathrm{m^2/V}$ and number of charge carriers $p = 1/(R_H q) = 3 \times 10^{26}\ \mathrm{m^{-3}};\ 2 \times 10^{26}\ \mathrm{m^{-3}}$ correspondingly at 2 K and 300 K for 25 nm nanoflake, where $R_H = (R_{xy}d)/B$ is Hall coefficient, ρ is the resistivity of the sample and q is the elementary charge. The concentration of holes in 25 nm nanoflake exceeds the concentrations typically observed in the bulk Sb_2Te_3. Note that due to nonlinear behavior of $R_{xy}(B)$ there is no definite value of the mobility and the number of charge carriers for 450 nm sample and both parameters μ and p become dependent on the magnetic field.

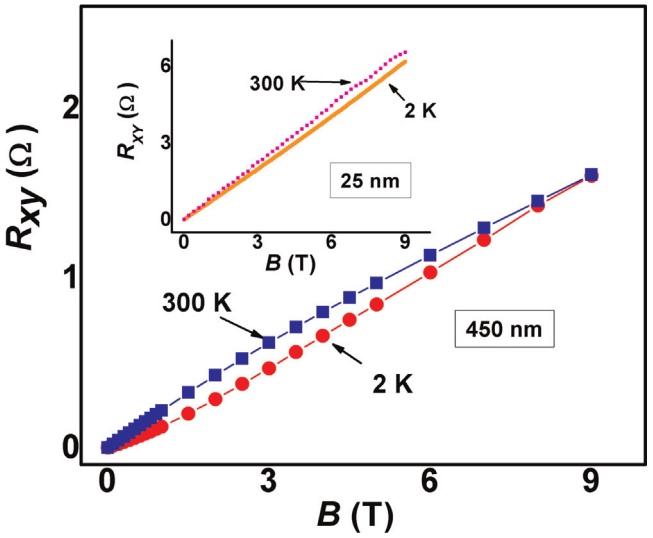

Fig. 2. The magnetic field dependence of the transverse resistance R_{xy} of Sb_2Te_3 nanoflakes.

Fig. 3 represents MR of both nanoflakes at 2 K and 300 K temperatures. While 25 nm sample demonstrates ordinary positive magnetoresistance (quadratic dependence $\sim(\mu B)^2$) throughout the range of applied magnetic fields and temperatures, the magnetoresistance of 450 nm sample is quadratic only at low fields < 1.5 T. In the high fields the longitudinal resistance $R_{xx}(B)$ of 450 nm sample behaves as $\sim B^{0.35}$ at 2 K and is linear $\sim B$ at 300 K (see Fig. 4). The sense of curvature of the $R_{xx}(B)$ line (as in the case

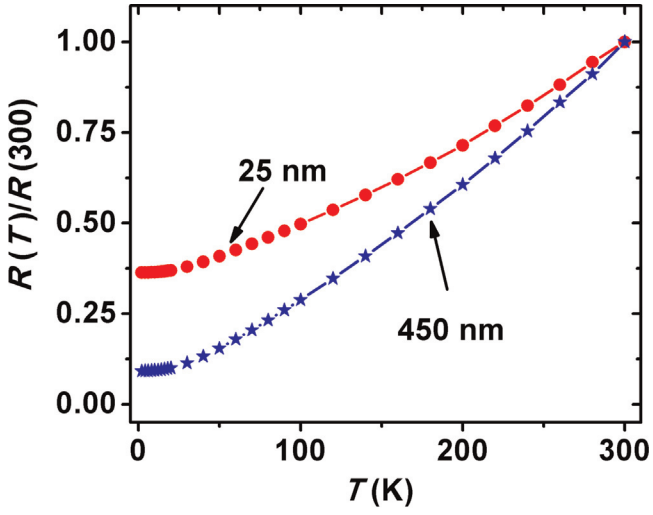

Fig. 1. The temperature dependences of normalized resistance $R(T)/R(300\ \mathrm{K})$ of Sb_2Te_3 nanoflakes.

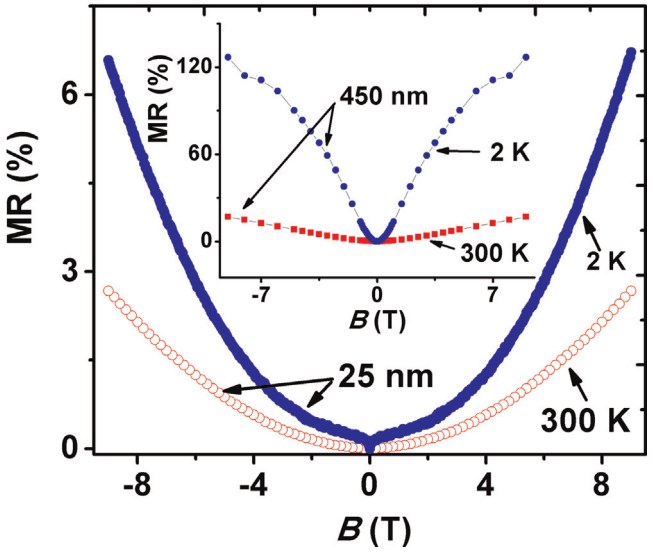

Fig. 3. The magnetoresistance of Sb_2Te_3 nanoflakes at 2 K and 300 K.

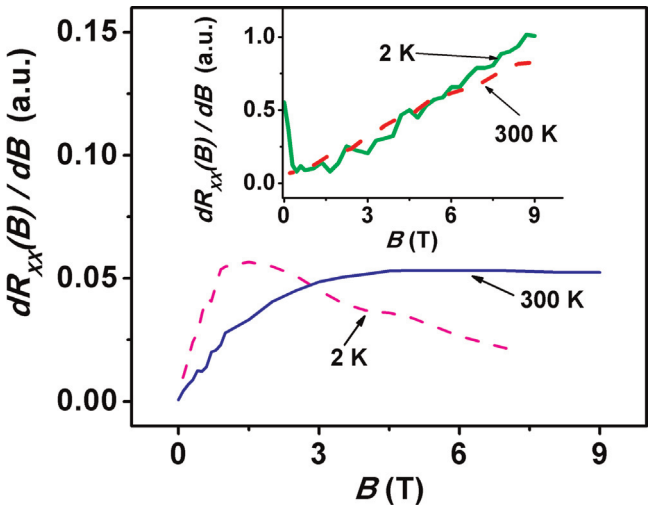

Fig. 4. The first derivative of the longitudinal resistance R_{xx} of the 450 nm and 25 nm samples (inset).

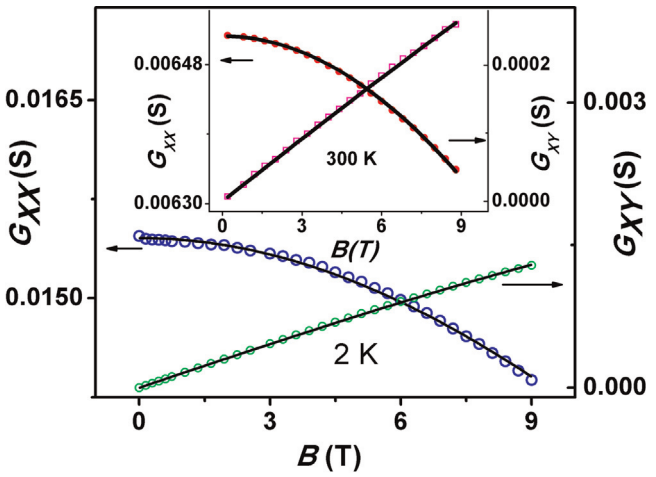

Fig. 5. The extracted magnetoconductance components $G_{xx}(B)$ and $G_{xy}(B)$ of the 25 nm sample. The solid lines are the fitting curves.

of $R_{xy}(B)$ dependence) is reversed at 300 K. Besides, the thinner nanoflake exhibits an anomaly at zero field and 2 K, which is absent in the case of 450 nm sample. The anomaly is presumably related to WAL effect inherent for topological insulators and, as it was mentioned above, has been observed in other thin TIs. The WAL effect (associated with the surface states) usually is not detected in the thick samples (as in the case of our 450 nm sample), because the relative contribution of the surface states decreases with increasing the thickness of the samples. The anomaly is smeared and is not observed at 300 K due to the decrease of the phase coherence length (which is ~300 nm at 2 K) at higher temperature [10]. An additional electron-phonon scattering at high temperatures reduces the mobility of the charge carriers and leads to decrease of the magnitude of the magneto-resistance at room temperature. Some dispersion observed at high fields on MR curve of 450 nm sample is, presumably, the result of Shubnikov-de Hass oscillations which are intensified with the field.

3. Results and discussions

A study of the obtained behaviors of the magnetoresistance and Hall resistance of the nanoflakes can be made by considering R as a function of the appropriate components of the magneto-conductivity tensor, which for the case of the electric field in the X direction and B in the Z direction are

$$R_{xx} = \frac{G_{xx}}{G_{xx}^2 + G_{xy}^2},\ R_{xy} = \frac{G_{xy}}{G_{xx}^2 + G_{xy}^2} \tag{1}$$

$$G_{xx} = \frac{R_{xx}}{R_{xx}^2 + R_{xy}^2},\ G_{xy} = \frac{R_{xy}}{R_{xx}^2 + R_{xy}^2} \tag{2}$$

where G_{ij} are magnetoconductivity components. First, we extracted the experimental dependencies of $G_{xx}(B)$ and $G_{xy}(B)$ taking into account the expressions (2). Next, in case of 25 nm sample, applying the expressions of Drude model

$$G_{xx} = \frac{qp_f\mu_f}{[1 + (\mu B)^2]},\ G_{xy} = \frac{qp_f\mu_f^2 B}{[1 + (\mu B)^2]} \tag{3}$$

to the experimental $G_{ij}(B)$ curves the fitting parameters of μ_f and p_f were obtained. The fits yield good agreement with the measured magnetoresistance and Hall resistance (see Fig. 5). The extracted values of the mobility μ_f=0.03 m^2/V and the number of charge carriers $p_f = 1.8 \times 10^{26}$ m^{-3} at 2 K and μ_f=0.0186 m^2/V, $p_f = 1.2 \times 10^{26}$ m^{-3} at 300 K agree well to experimental values in orders, as well as repeat the trend with temperature. Unfortunately, parameters extracted from the Hall conductivity $G_{xy}(B)$ did not match what is found from the magnetoconductivity $G_{xx}(B)$. The disagreement between parameters of $G_{xy}(B)$ and $G_{xx}(B)$ is common in semiconductors and arises from the fact that scattering mechanisms are not energy independent. Thereby, the measured Hall mobility and the Hall carrier density would differ from the actual electron drift mobility and carrier density through a multiplicative scattering factor $r = \langle\tau^2\rangle/\langle\tau\rangle^2$, with τ being the mean time between carrier collisions [24].

The non-linear Hall effect observed in 450 nm sample is a signature of multichannel transport, implying coexistence of parallel channels. Therefore, we apply a two-channel model with the same p-type of charge carriers but of different density and mobility. The nature of the origin of the carriers with different density and mobility is not identified. In TIs it is usually ascribed to coexistence of the bulk charge carriers and carriers of the surface states. However we cannot exclude the contribution of both the upper valence band with light effective mass holes and lower valence band with heavy effective mass holes. Thus, the total conductivity is the sum of the conductivities of the two channels $G = G_1 + G_2$.

$$G_{xx} = \frac{qp_f^{(1)}\mu_1}{[1 + (\mu_1 B)^2]} + \frac{qp_f^{(2)}\mu_2}{[1 + (\mu_2 B)^2]},\ G_{xy} = \frac{qp_f^{(1)}\mu_1^2 B}{[1 + (\mu_1 B)^2]} + \frac{qp_f^{(2)}\mu_2^2 B}{[1 + (\mu_2 B)^2]} \tag{4}$$

Here, $p_f^{(i)}$ is an effective carrier density and μ_i is the mobility of the i-th channel for the i=1 and 2 conduction channels. Applying the expressions (4) to the experimental $G_{ij}(B)$ curves the fitting parameters of μ_i and $p_f^{(i)}$ for each channel were obtained. As shown in Fig. 6 the fits yield a good agreement with experimental data. The obtained parameters are μ_1=0.63 m^2/V, $p_f^1 = 5.9 \times 10^{25}$ m^{-3}, μ_2 = 0.1 m^2/V, $p_f^2 = 0.8 \times 10^{25}$ m^{-3} at 2 K and μ_1=0.26 m^2/V, $p_f^1 = 0.24 \times 10^{25}$ m^{-3}, μ_2=0.065 m^2/V, $p_f^2 = 4.5 \times 10^{25}$ m^{-3} at 300 K. Here, we have to say that, as in the case of 25 nm sample, the parameters obtained from the magneto-conductivity and the Hall conductivity do not coincide. The comparison of fitting parameters μ and p of two nanoflakes shows that actually the resistance of 450 nm sample have to be lower than the resistance of 25 nm sample due to considerably higher mobility and lower density of charge carriers (what is confirmed by $R(T)$ data, see Fig. 1). Next,

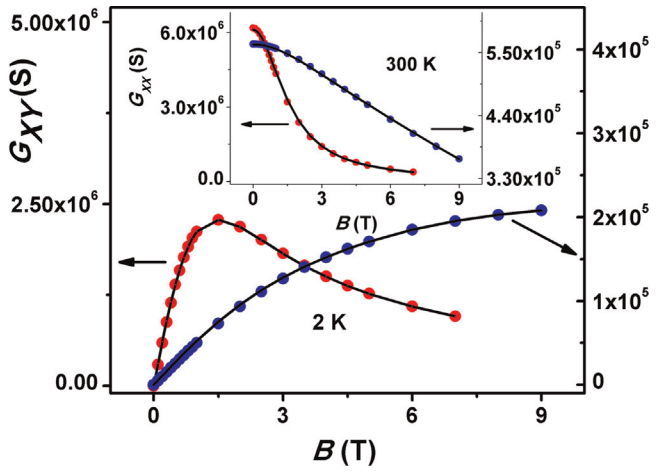

Fig. 6. The extracted magnetoconductance components $G_{xx}(B)$ and $G_{xy}(B)$ of the 450 nm sample. The solid lines are the fitting curves.

what we have noticed is that the majority carriers at 2 K are the carriers with high mobility, but at 300 K the majority carriers are the carriers with low mobility. And we consider this inversion between the densities of the majority and minority carriers as the principal cause of the changes of the sense of curvature of both $R_{xy}(B)$ and $R_{xx}(B)$ dependences. The strong electron-phonon scattering causes drastic decrease of the density of the high mobility carriers at high temperature. The condition existing in 450 nm sample at 300 K may roughly be compared with the condition in 25 nm sample even at 2 K. The scattering of charge carriers in 25 nm sample is so strong (because of the huge number of defects) that suppresses the number of high mobility carriers to the negligible amount, which in its turn, leads to the ordinary magnetoresistance and Hall effect. And the results have allowed us to analyze 25 nm sample in the model with single channel transport. Comparing the behavior of the Hall resistances R_{xy} of both 25 nm and 450 nm samples we can conclude that the nonlinear behavior of $R_{xy}(B)$ is not related to the surface states, otherwise, the effect would be stronger for 25 nm sample. Note, that observing WAL effect (which may be a response of the surface states) in the magnetoresistance of 25 nm sample it would be reasonable to expect some effect of the surface states on Hall resistance too. We can suppose that even if the effect exists it is masked by the background of the strong scattering processes. Therefore, we inclined to attribute the existence of two channel transport in the samples to the contribution of both valence bands with light and heavy effective mass holes. The used models does not take into account the spin-dependent current (or the spin-dependent scattering) which in the case of strong spin–orbit coupling is not negligible. Possibly, the obtained mismatch between the two groups of parameters μ_f and p_f obtained from the $G_{xy}(B)$ and $G_{xx}(B)$ data is also related to this deficiency of the applied model.

4. Conclusion

Single crystal Sb_2Te_3 topological insulator nanoflakes with the thickness of 25 nm and 456 nm were synthesized via vapor phase deposition method. The Hall resistance and magnetoresistance of the nanoflakes have been measured at temperatures 2 K and 300 K in the fields up to 9 T. The magnetoresistance and Hall resistance of the nanoflakes demonstrate considerably different behaviors, in particular, despite ordinary MR and Hall effect obtained for 25 nm sample 450 nm nanoflake demonstrates unusual MR and nonlinear Hall resistance and the sense of curvature of both $R_{xx}(B)$ and $R_{xy}(B)$ dependences is inversed at the high temperature. The experimental data have been analyzed in the frame of a multi-channel transport model. The difference in the behaviors is attributed to the existence of the charge carriers with high and low mobility, as well as their relative contribution (which varies depending on the temperature) to the magneto-transport of the nanoflakes. However, the nature of the origin of the same type of charge carriers but with different values of mobility is still unclear. Additional measurement on different single crystal Sb_2Te_3 nanoflakes with lower concentration of charge carriers will be needed to carry out. The concentration of the charge carriers can be reduced by controlling the Sb/Te ratio.

Acknowledgments

Authors thank Dr. Pai-Chun Wei for providing us with Sb_2Te_3 ingot, Wei-Chiao Lai; Prof. Chia-Seng Chang for support on AFM measurement, and Drs. V. Mekhitaryan and V. Mkrtchian for fruitful discussions. The work was supported by National Science Council Taiwan, under Grant #NSC100-2112-M-001-019-MY3, Armenia State Base Funding Project E-5 and technical support from Core Facility for Nanoscience and Nanotechnology at Academia Sinica in Taiwan.

References

[1] M.Z. Hasan, C.L. Kane, Rev. Mod. Phys. 82 (2011) 3045.
[2] J.E. Moore, Nature 464 (2010) 194.
[3] Yoichi AndoS.-C. Zhang, Physics 1 (2008) 6s.
[4] S.S. Hong, J.J. Cha, D. Kong, Y. Cui, Nat. Commun. 3 (2012) 756.
[5] S. Matsuo, T. Koyama, K. Shimamura, T. Arakawa, Y. Nashihara, D. Chiba, K. Koboyashi, T. Ono, C.-Z. Chang, K. He, X.-C. Ma, Q.-K. Xue, Phys. Rev. B 85 (2012) 075440.
[6] L. Bao, L. He, N. Meyer, X. Kou, P. Zhang, Z.-G. Chen, A.V. Fedorov, J. Zou, T. M. Riedemann, T.A. Lograsso, K.L. Wang, G. Tuttle, F. Xiu, Sci. Rep. 2 (2012) 726.
[7] J.H. Bardarson, J.E. Moore., Rep. Prog. Phys. 76 (2013) 056501.
[8] Bacel Hamdou, Johannes Gooth, August Dorn, Eckhard Pippel, Kornelius Nielsch, Appl. Phys. Lett. 102 (2013) 223110.
[9] Y. Takagaki, A. Giussani, K. Perumal, R. Calarco, K.-J. Friedland, Phys. Rev. B. 86 (2012) 125137.
[10] Yi-Chi Huang, P.C. Lee, C.H. Chien, F.Y. ChiuY.Y. ChenSergey R. Harutyunyan, Physica B 452 (2014) 108.
[11] D.X. Qu, Y.S. Hor, J. Xiong, R.J. Cava, N.P. Ong, Science 329 (2010) 821.
[12] Z.J. Yue, X.L. Wang, Y. Du, S.M. Mahboobeh, F.F. Yun, Z.X. Cheng, S.X. Dou, EPL 100 (2012) 17014.
[13] H. Tang, D. Liang, R.L.J. Qiu, X.P.A. Gao, ACS Nano 5 (2011)7510 5 (2011).
[14] H. He, B. Li, H. Liu, X. Guo, Z. Wang, M. Xie, J. Wang, Appl. Phys. Lett. 100 (2012) 032105.
[15] Heon-Jung Kim, Ki-Seok Kim, Mun Dae Kim, S.-J. Lee, J.-W. Han, A. Ohnishi, M. Kitaura, M. Sasaki, A. Kondo, K. Kindo, Phys. Rev. B 84 (2011) 125144.
[16] A.A. Abrikosov, Quantum linear magnetoresistance, . Europhys. Lett. 49 (2000) 789.
[17] B.A. Assaf, T. Cardinal, P. Wei, F. Katmis, J.S. Moodera, D. Heiman, Appl. Phys. Lett. 102 (2013) 012102.
[18] Naoto Nagaosa, Jairo Sinova, Shigeki Onoda, A.H. MacDonald, N.P. Ong, Rev. Mod. Phys. 82 (2010) 1539.
[19] J. Zhang, C.-Z. Chang, Z. Zhang, J. Wen, X. Feng, K. Li, M. Liu, K. He, L. Wang, X. Chen, Q.-K. Xue, X. Ma, Y. Wang, Nat. Commun. 2 (2011) 574.
[20] H. Zhang, Ch-H. Liu, X.-L. Qi, X. Dai, Zh Fang, Sh-Ch Zhang, Nat. Phys. 5 (2009) 438.
[21] V.A. Kulbachinskii, A. Yu., R.A. Kaminsky, K. Lunin, Y. Kindo, K. Narumi, S. Suga, M. Kawasaki, N. Sasaki, P. Miyajima, Lostak, P. Hajek, Semicond. Sci. Technol. 17 (2002) 1133.
[22] Y. Takagaki, B. Jenichen, U. Jahn, M. Ramsteiner, K.-J. Friedland, J. Lahnemann, Semicond. Sci. Technol. 26 (2011) 125009.
[23] Hui Li, Jie Cao, Wenshan Zheng, Yulin Chen, Di Wu, Wenhui Dang, Kai Wang, Hailin Peng, Zhongfan Liu, J. Am. Chem. Soc. 134 (2012) 6132.
[24] Dieter K. Schroder, Semiconductor Material and Device Characterization, 3rd ed., IEEE Press, John Wiley & Sons, Inc., Hoboken, New Jersey, 2006.